

Spectral evolution of nano-second laser interaction with Ti target in nitrogen ambient gas

H. Hegazy · H. A. Abd El-Ghany · S. H. Allam ·
Th. M. El-Sherbini

Received: 31 October 2013 / Accepted: 9 April 2014 / Published online: 7 May 2014
© Springer-Verlag Berlin Heidelberg 2014

Abstract The present work aimed to study the variation in the plasma parameters (temperature and density) of the Ti plasma generated by 1,064 and 532 nm lasers at different ambient N₂ pressures for different delay times. The characterization of the plasma-assisted pulsed laser ablation of the titanium target is discussed. The emission spectra of the titanium plasma produced in the present study have been carefully investigated over the whole UV–NIR (200–1,000 nm) spectral range. Boltzmann plots of suitable spectral lines have been employed to derive the excitation temperature, and the electron density is derived from the Stark widths of the Ti II spectral line at 350.49 nm.

1 Introduction

Over the past few years, the interaction of laser light with solid targets and the consequently produced plasma have been studied [1–4]. Despite great efforts to exploit laser

matter interaction for material processing and diagnostic purposes, many aspects still need to be elucidated and clarified [5]. Plasmas induced by nanosecond lasers are successfully employed for thin-film deposition over a wide range of classical and novel materials [6] and for in situ qualitative elemental analysis [7, 8]. Pulsed laser deposition (PLD) has emerged as a very versatile, flexible, and efficient procedure for obtaining high-quality thin layers [9–11]. When PLD is carried out in the atmosphere of a reactive gas, the flux of laser-ablated material interacts with the gas molecules all along the transit from the target to the collector surfaces [12–14]. The deposited layer consists of a chemical compound that is considerably different from the base material. The plasma produced by PLD using short laser pulses has been shown to be an efficient tool to produce small particles in the nanometer size range [15–17]. However, little is known about the physical mechanisms involved in the particle formation. Recently, molecular dynamic simulations have been used to analyze short-pulse laser ablation [18]. The calculations predict plume composition, kinetic energies of species, and the size distribution of nanoparticles at the early stage of plume expansion. However, experimental results suitable for the validation of these theoretical findings are still lacking.

Surface modification of titanium to improve its wear resistance has been the subject of a number of investigations including the use of high-power lasers [19–25]. Laser surface nitriding in particular is an attractive process because of its simplicity and the possibility of producing hard layers of substantial depths (>1 mm) with minimum effect to the “bulk” of the material [26]. Laser surface nitriding was initiated by the work of Katayama et al. [21], and since then, there have been a number of other investigations. The process involves using the intense optical

H. Hegazy (✉)
Physics Department, Faculty of Science, Jazan University,
Jazan 2079, Saudi Arabia
e-mail: hossamhegazy@Jazanu.edu.Sa

H. Hegazy
Plasma Physics Department, NRC, Atomic Energy Authority,
Enshass 13759, Egypt

H. A. Abd El-Ghany
Department of Engineering Mathematics and Physics, Faculty
of Engineering, Banha University, Cairo, Egypt

S. H. Allam · Th. M. El-Sherbini
Laboratory of Lasers and New Materials, Department of Physics,
Faculty of Science, Cairo University, Cairo, Egypt

energy of the laser to melt the surface in a nitrogen-containing atmosphere. Extensive and rapid solution of nitrogen in molten titanium occurs, and dendrites of TiN are produced at traverse speeds of the order of 100 mm/s [22]. As in all laser surface modification processes, surface layers are produced by overlapping of single melt tracks.

The surface of titanium targets can be modified by a variety of laser treatments carried out in ambient gases, and different compounds are likely to be formed [27]. Nitrides are considered one of the most important titanium compounds for their interesting properties [28–30], which exhibit properties characteristic of both covalent and metallic compounds [31]. Titanium nitride coatings obtained by laser modification techniques have been used for the production of high-performance coatings with increased corrosion resistance [32–34], improved machining tools [35–37], biocompatible coatings [38], and increased wear resistance in tribology applications [39–42]. In addition, they have exhibited optical properties, which make them attractive candidates for decorative coatings [43]. The latter have specifically been suggested for TiO_x coatings obtained with a similar laser technique [44]. Its very good electrical conductivity and excellent performance as an adhesion layer make TiN an interesting material for microelectronic applications, e.g., as a diffusion barrier between silicon substrates and aluminum metallizations [45, 46].

The applications of titanium and its alloys are numerous. Due to its high strength to weight ratio, it is used in airplane parts, fasteners [47], and gas turbine engines [48] and for parts such as the compressor blades, casings, engine cowlings, and heat shields. Since titanium has good corrosion resistance, titanium's resistance to chlorine and acid makes it an important material in chemical processing [49]. One of the most notable recent uses of titanium is in artificial hearts first implanted in a human in 2001 [50]. Finally, titanium materials are used in the production of numerous consumer products. It is used in the manufacture of such things as shoes, jewelry, computers, sporting equipment, and watches [51, 52].

As mentioned above, plasma plays an essential role in determining the characteristics of the deposited layers in PLD and on surface modification of titanium to improve its wear resistance. Precise knowledge of the electron temperature and electron density is a necessary requirement for better understanding the basic plasma processes as plasma dynamics, heat conduction, melting, vaporization of solid targets, and development of the mechanisms of excitation and recombination process in laser plasmas. The excitation temperature is often determined from the relative intensities of some suitable optically thin spectral lines with small separation in wavelength but wide separation in the excitation energies. The derivation of the electron density from line profiles requires well-isolated and optically thin

spectral lines affected by the plasma electric field, which results in broadening of the lines.

In continuation of previous investigations [53], the present work aimed to study the variation in temperature and density of the Ti plasma generated by 1,064 and 532 nm lasers at different ambient N₂ pressures for different delay times.

2 Experimental setup

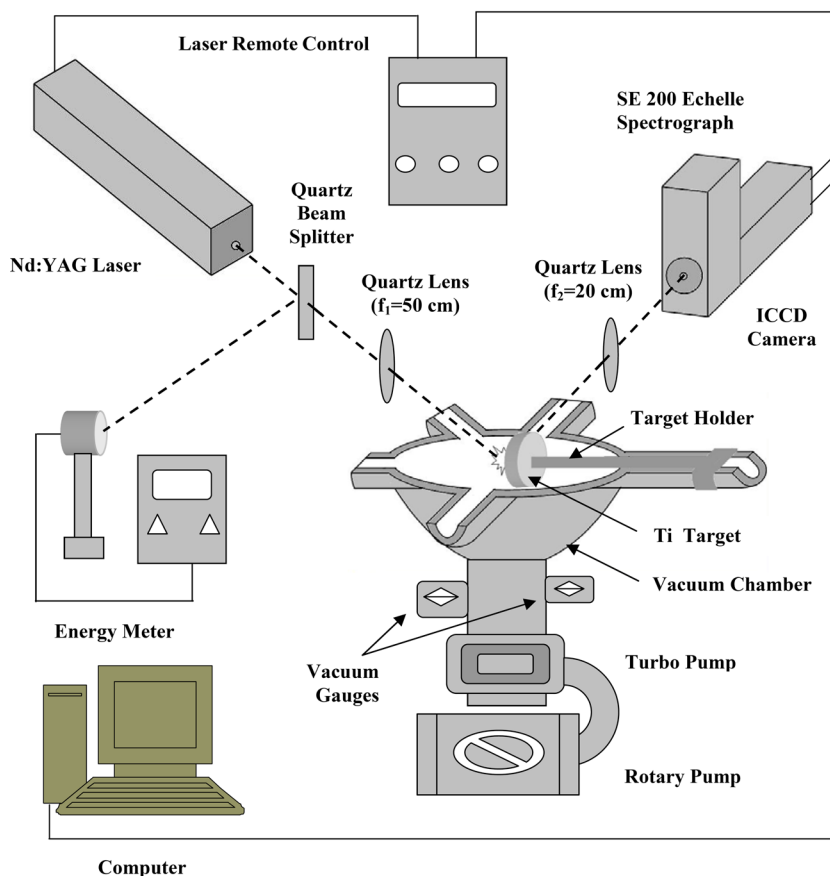
A schematic diagram of the experimental setup is shown in Fig. 1. The experiments are performed in such a way that a Q-switched Nd:YAG laser [type Brilliant B from Quantel] is used for producing the titanium plasma at the fundamental wavelength (i.e., $\lambda = 1,064$ nm) and at the second harmonic wavelength (i.e., $\lambda = 532$ nm).

The laser beam is focused onto the target using a quartz lens ($f_1 = 50$ cm) at 45°; however, the lens position is optimized and readjusted for obtaining the best focus for both laser wavelengths. The calculation of the power density and the focal spot radius was done using the relation $w_2 \approx 2.44 \lambda \frac{f}{w_1}$ [53], where w_1 is the diameter of the laser beam before focalization (≈ 1 cm), w_2 is the diameter of laser beam at the focus; f is the focal length of the lens, and λ is the laser wavelength. In the present work, the laser energy per pulse is 490 mJ in 6 ns and 200 mJ in 5 ns at the target surface for a laser focal spot of 0.65 and 0.32 mm for the fundamental and second harmonic wavelengths, respectively. This corresponds to irradiance on the target of 0.6×10^{12} W/cm² for the fundamental wavelength and of 1.2×10^{12} W/cm² for the second harmonic wavelength. The calculated spot size is consistent with the visual observation of the target spots.

A quartz beam reflector is used for monitoring the reproducibility of the incidence laser beam energy on the target, which partially reflects about 6 % of the incident laser energy to an absolutely calibrated energy meter-type Ophir model 1Z02165. The target is mounted in a stainless steel vacuum chamber with the aid of a rotating target holder, which is slowly rotated to provide a fresh surface after each laser pulse and to avoid a deep crater. The chamber is evacuated down to $<6 \times 10^{-6}$ Torr using a turbo molecular pump backed by an oil-sealed mechanical rotary pump.

The plasma emission is collected in the direction parallel to the target surface (side-on view) with the aid of a quartz lens of focal length ($f_2 = 20$ cm); the lens is positioned to produce a 1:1 image of the plasma plume at the entrance aperture of an Echelle spectrograph [type Catalina Corp, model SE 200]. The instrument is coupled to an intensified charge-coupled device (ICCD) camera [type Andor, model iStar DH734-18F]. The entrance aperture of a spectrograph is a circular opening 50 μ m in diameter, and

Fig. 1 Schematic diagram of the experimental setup



the ICCD is contained in a camera head mounted at the exit port. The emission from the plasma is collected by scanning the spectrograph over the wavelengths of interest. The system is fed by KestrelSpec software to acquire images from the supported camera, align and focus the images, calibrate and analyze the spectral data. The system of detection covers a wavelength range from 200 to 1,000 nm with a constant resolution of $\Delta\lambda/\lambda = 4,500$ over three points. An Oriel low-pressure Hg pin lamp is used for wavelength calibration. The spectra are acquired at different delays after the laser pulse, using constant opening gates of the ICCD (2 μ s). The choice of the gate corresponds to a compromise between the need of not having very large variations in the signal during the measurement time, and at the same time having a good signal for calculating line intensities and widths. The experimental measurements are collected from three different single shots for three different “fresh targets”; this allows us to present an average and a standard deviation of the results.

3 Results and discussions

The study of the emission from the titanium plasma generated by the lasers at the wavelengths of 532 and 1,064 nm at

different N_2 ambient gas pressures for different delay times reveals that the continuum at the initial stage decreases with the increase of the delay time. The emission spectrum of the plasma consists mainly of transition lines of Ti I and Ti II, covering the range of (200–1,000 nm). At lower ambient pressure values, the intensities of Ti spectral lines last only for a few hundreds of nanoseconds even not more than 500 ns at 15 Torr. As the ambient pressure gets higher, the lines can last for up to several microseconds and even reach about 25 μ s at 760 Torr.

Figures 2 and 3 show the spectral distribution of Ti II spectral lines at 321.71, 325.29, and 350.49 nm for different delay times, while Figs. 4 and 5 show the variation in the emission intensity of the Ti II spectral lines at 321.71, 325.29, and 350.49 nm generated by the lasers of wavelengths 532 and 1,064 nm for different pressures of N_2 ambient gas. These results reveal that the intensities of the Ti II spectral lines are much higher for the plasma generated by the 1,064 nm laser than for the 532 nm laser for different pressures of N_2 ambient gas. We should mention that the higher intensity of the spectral line may be attributed to stronger ablation of the sample. The mass ablation of the metal depends upon the thermodynamic and optical properties of the sample as well as on the laser properties (wavelength, pulse duration, and irradiance).

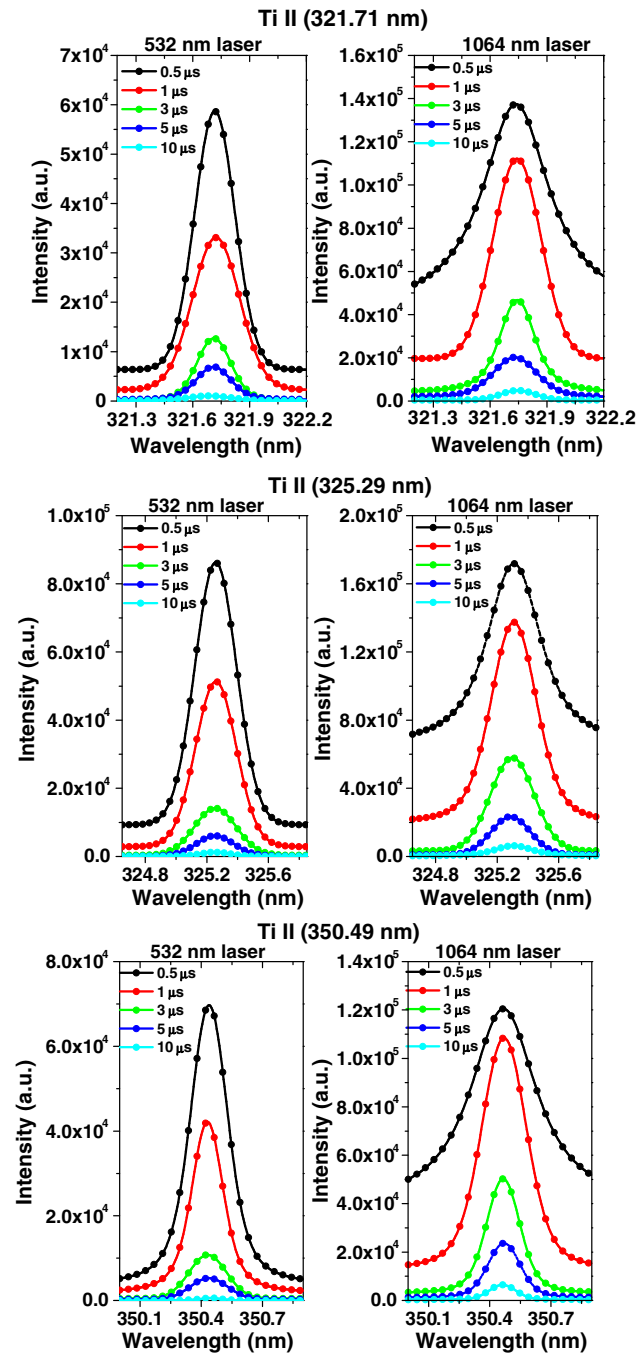


Fig. 2 Spectral distribution of Ti II lines at 321.71, 325.29, and 350.49 nm emitted from the plasma generated by laser wavelengths of 532 and 1,064 nm at 350 Torr of ambient N_2 gas at different delay time

The effect of the ambient atmosphere (N_2) plays a dominant role in the mass ablation rate with the incident laser beam properties. In the model introduced by Fornarini et al. [54], the interactions between the incoming radiation and the solid sample depend upon numerous variables related to the laser, the sample, and the surrounding atmosphere. These variables include wavelength, energy, spatial and

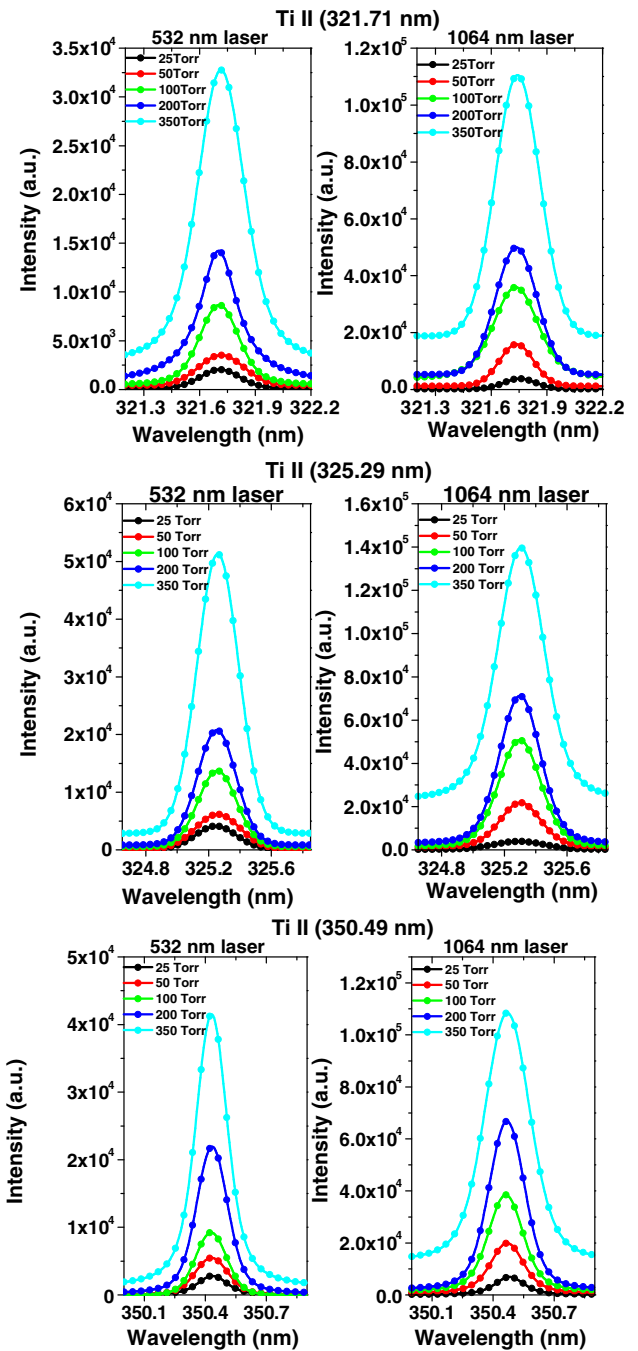


Fig. 3 Spectral distribution of Ti II lines at 321.71, 325.29, and 350.49 nm emitted from the plasma generated by laser wavelengths of 532 and 1,064 nm at $t_d = 1 \mu s$ for different pressures of ambient N_2 gas

temporal profile of the laser beam, and the thermal properties of the sample. The incident beam is partially reflected by the sample surface and partially absorbed by the bulk to a degree that depends on the nature of the target and the temperature it reaches under laser irradiation. The rate of the radiation–solid interaction is also known to depend on the laser wavelength [54].

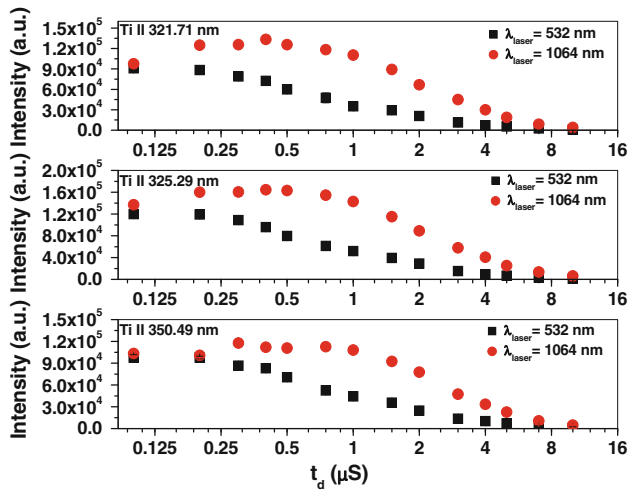


Fig. 4 Variation in the emission intensity of Ti II lines at 321.71, 325.29, and 350.49 nm emitted from the plasma generated by laser wavelengths of 532 and 1,064 nm at 350 Torr of ambient N_2 gas versus the delay times

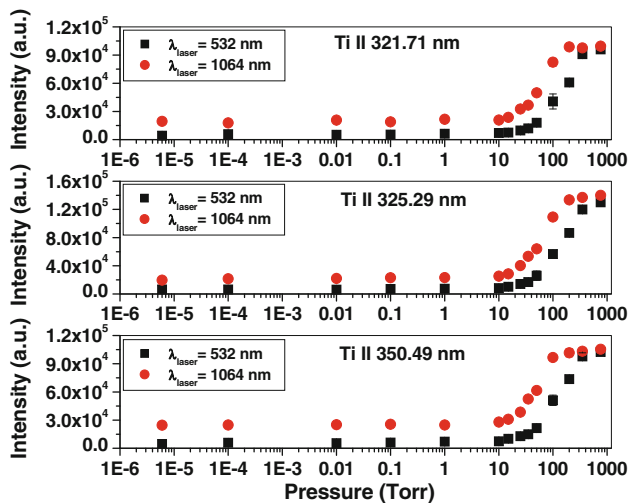


Fig. 5 Variation in the emission intensity of Ti II lines at 321.71, 325.29, and 350.49 nm emitted from the plasma generated by laser wavelengths of 532 and 1,064 nm at $t_d = 1 \mu s$ for different pressures of ambient N_2 gas

For evaluating the plasma parameters and extracting quantitative data from the line intensities, it is important to verify that the plasma is not optically thick for the lines being used for this purpose. The ratio of emission intensities of resonant and nonresonant lines was verified according to a procedure for the “optically thin” limit described by *Cremers and Radziemski* [55], *Simeonsson and Miziolek* [56], and *Sabsabi and Cielo* [57]. The absence of self-absorption is a necessary requirement for a spectral line to be used in the calculations of the excitation temperature and the electron density in the produced plasma.

A multiplet is very useful in the assessment of self-absorption [53, 58, 59]. Testing the self-absorption of Ti I

spectral emission lines reveals that all Ti I spectral lines are affected by self-absorption. By examining the intensity ratio of the doublet lines of the transition $3d^2(^3F) 4s-3d^2(^3F) 4p$ of Ti II at 321.71 nm and Ti 325.29 nm [53], the calculated optically thin limit was found to be 1.35. The experimental measured ratio agreed with this limit within acceptable error bars for different delay times. Recalling the fact that transitions not ending in the ground state are hardly affected by any self-absorption [58]; it can be concluded that the spectral lines arising from transitions between the same or higher energy levels are all free of self-absorption for the present experimental conditions.

Due to the short plasma life time at lower N_2 pressures, the emission intensity of one of the Ti II spectral lines at $\lambda = 348.36$ nm used for temperature measurements becomes very weak, and the excitation temperature can be calculated for just a few hundreds of nanoseconds at the lower values of ambient N_2 pressures, i.e., at 25 Torr, it can be calculated up to 1.5 and 3 μs for plasmas produced by the 532 nm and 1,064 nm lasers, respectively. As the ambient N_2 pressure gets higher, the calculation of the excitation temperature can be performed for several microseconds ($\geq 10 \mu s$ at 760 Torr). However, measurements of the electron density from the Stark width of the line profile of the Ti II spectral line at $\lambda = 350.49$ nm are possible up to 10 μs for lower pressures, and as the N_2 pressure gets higher, the density can be performed up to 25 μs at 760 Torr.

4 Measurements of plasma temperature

In LTE or near LTE, the relative intensities of spectral lines solely depend on the electron temperature since the population densities of the upper levels follow a Boltzmann distribution. The intensity of a spectral line thus is given by [60, 61]:

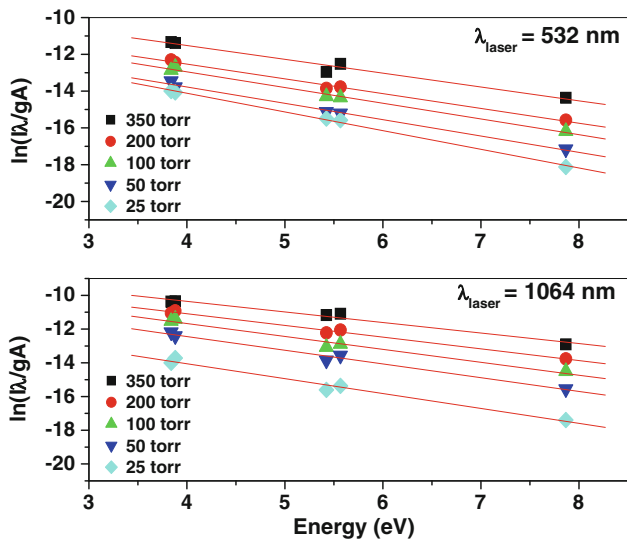
$$I_{ij} = \frac{L}{4\pi} h\nu g_i A_{ij} \frac{N_o}{U(T)} \exp\left(-\frac{E_{exc}}{k_B T_{exc}}\right), \quad (1)$$

where $U(T)$ is the partition function, L is the plasma length, A_{ij} is the transition probability, g_i is the statistical weight of the upper level, N_o is the number density of atoms in the ground state, T_{exc} is the excitation temperature \sim electron temperature, and E_{exc} is the excitation energy of the upper level. By plotting $\ln(I \lambda/gA)$ versus E_{exc} , the so-called Boltzmann plot is obtained. In LTE, it is a straight line with the slope equal to $-(1/k_B T)$.

In the present work, the temperature of the generated titanium plasma has been calculated using Boltzmann plots of the well-developed five Ti II spectral lines for which we had proved their accuracy and stability for temperature measurements [53]. The spectroscopic atomic data of these

Table 1 The spectroscopic atomic data of the Ti II spectral lines used in calculations

λ_{ki} (nm)	E_i (eV)	E_k (eV)	g_i	g_k	A_{ki} (S^{-1})
286.23	1.2369	5.5672	4	6	4×10^7
321.71	0.0279	3.8808	8	10	1.69×10^7
325.29	0.0279	3.8384	8	10	3.83×10^7
348.36	4.3083	7.8663	10	8	9.7×10^7
351.08	1.8927	5.4232	8	8	9.25×10^7

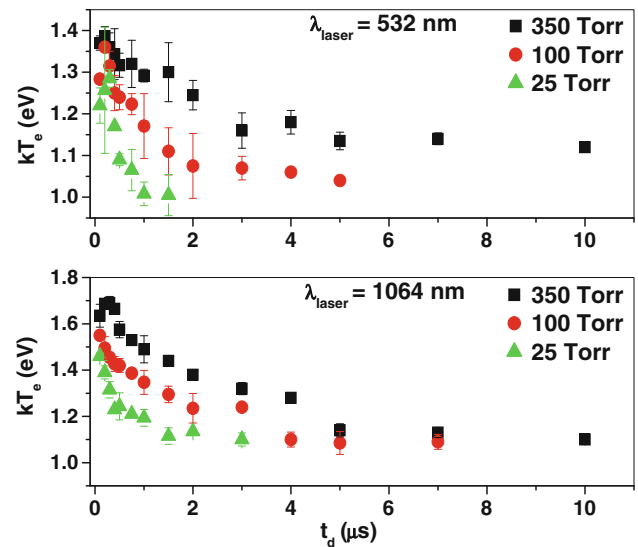
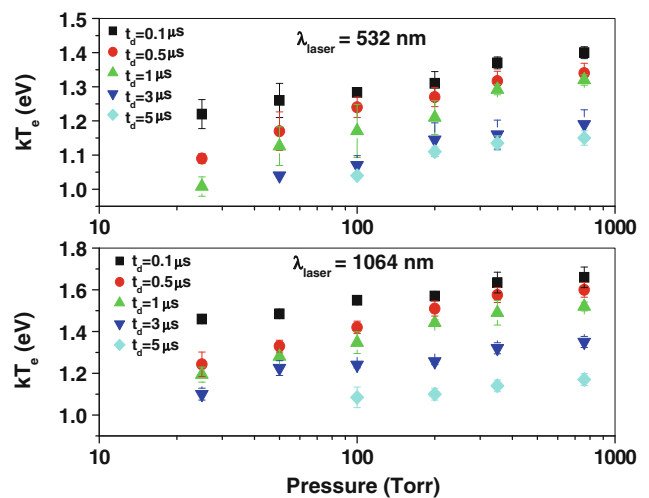
**Fig. 6** Boltzmann plots at different pressures of the ambient N_2 gas for the plasma generated by 532 and 1,064 nm lasers at $t_d = 1 \mu s$

Ti II spectral lines are presented in Tables 1 [62]. Since the wavelength interval between the selected spectral lines is not small enough, a correction of their intensities is necessary. The necessary correction has been performed using the sensitivity calibration curve obtained by a deuterium–tungsten–halogen lamp.

Figure 6 shows typical Boltzmann plots at different pressures of ambient N_2 gas for the plasma generated by the 532 nm and 1,064 nm lasers. The regression was between (0.966 and 0.999) for different experimental operating conditions.

The temporal evolution of the temperature at different N_2 ambient pressures for the titanium plasmas generated by the lasers of wavelengths of 532 and 1,064 nm shows that the temperature is considerably high at the initial stage of the plasma, and then, it decreases quickly with the delay time as shown in Fig. 7.

Figure 8 shows the variation in the excitation temperature with different N_2 ambient pressures at different delay times for the titanium plasma generated by the laser wavelengths of 532 and 1,064 nm. It can be noticed that the excitation temperature increases with increasing the

**Fig. 7** Temporal variation in the plasma temperature for the Ti plasma generated by 532 and 1,064 nm lasers at different pressure of ambient N_2 gas**Fig. 8** Variation in the temperature for the Ti plasma generated by 532 and 1,064 nm lasers versus the ambient N_2 gas pressure determined for different time delays

pressure of the ambient N_2 gas. Moreover, the temperature decreases by increasing the delay time.

The measured temperature ranged from about 1.66 to 1.1 eV and from 1.4 to 1.12 in the delay time range (0.1–10 μs) for the plasmas produced by the 1,064 and 532 nm lasers, respectively, at atmospheric pressure of N_2 . At very low pressure (25 Torr), the corresponding temperature ranges were from 1.46 to 1.1 eV and from 1.22 to 1.01 eV. The detailed values for other pressures can be seen in Table 2; from the table, we also see that the plasma life time is low for lower N_2 pressures and increases as far as we reach the atmospheric pressure of N_2 ambient gas.

Table 2 Temperature values for plasma produced by both laser wavelengths at different delays

P (Torr)	Temperature (eV)													
	$t_d = 0.1 \mu s$		$t_d = 0.5 \mu s$		$t_d = 1.0 \mu s$		$t_d = 3.0 \mu s$		$t_d = 5.0 \mu s$		$t_d = 7.0 \mu s$		$t_d = 10 \mu s$	
	532 nm	1,064 nm	532 nm	1,064 nm	532 nm	1,064 nm	532 nm	1,064 nm	532 nm	1,064 nm	532 nm	1,064 nm	532 nm	1,064 nm
25	1.22	1.46	1.09	1.24	1.01	1.19	-	1.10	-	-	-	-	-	-
50	1.26	1.49	1.17	1.33	1.13	1.28	1.04	1.23	-	-	-	-	-	-
100	1.28	1.55	1.24	1.42	1.17	1.35	1.07	1.24	1.04	1.09	-	-	-	-
200	1.31	1.57	1.27	1.51	1.21	1.44	1.15	1.26	1.11	1.10	1.11	1.10	-	1.11
350	1.37	1.64	1.32	1.58	1.29	1.49	1.16	1.32	1.14	1.14	1.14	1.13	1.12	1.10
760	1.40	1.66	1.34	1.60	1.32	1.52	1.19	1.35	1.15	1.17	1.12	1.11	1.12	1.10

5 Measurements of plasma electron density

The measurement of the Stark broadening of spectral lines is considered the most powerful spectroscopic technique for determining the electron density of dense plasmas. This method is based on the assumption that the Stark effect is the dominant broadening mechanism, in comparison with Doppler broadening and other pressure broadening mechanisms due to collisions with neutral atoms (i.e., resonance and van der Waals broadening). The validity of this assumption was generally admitted in works on laser-induced plasmas and justified in various studies [55, 63, 64]. In case of well-isolated lines in neutral and singly ionized atoms, Stark broadening predominantly occurs by electron collisions. Since Stark broadening is rather weakly independent on the temperature, the electron density can be determined with good accuracy.

The FWHM of Stark-broadened lines is related to the electron number density [65, 66] and can be given by:

$$\Delta\lambda_{1/2} = 2W \frac{N_e}{10^{16}} \left[1 + 1.75A \left(\frac{N_e}{10^{16}} \right)^{\frac{1}{4}} \left(1 - \frac{3}{4} N_D^{-\frac{1}{3}} \right) \right], \quad (3)$$

where W is the electron impact parameter or Stark width parameter, A is the ion impact parameter, and N_D is the number of particles in the Debye sphere, which can be estimated from the relation: $N_D = 1.72 \times 10^9 \frac{T_e^{\frac{3}{2}}}{N_e^{\frac{1}{2}}} (4)W$ and A are functions of temperature and can be obtained by second order polynomials from [66].

In laser-induced plasmas with low temperature and high densities, the contributions by Doppler, van der Waals, and resonance broadenings are entirely very weak, so the second term of the Eq. (3) can be neglected. Then,

$$\Delta\lambda_{1/2} = 2W \frac{N_e}{10^{16}}. \quad (5)$$

In the present work, the Ti II spectral line at 350.49 nm was used for determining the electron density of the produced plasma [53]. The Stark width parameter of the Ti II spectral line of 350.49 nm has been experimentally determined by Hermann et al. [67, 68]. The least-square fit method to the profile is used to obtain the FWHM of this line. The measured instrumental width is 0.09 nm (determined from the FWHM of the Hg line at $\lambda = 280.35$ nm emitted by a standard low-pressure Hg lamp). Figure 9 presents an example of the line profile of the Ti II at $\lambda = 350.49$ nm with its best fit for the plasma generated by the 1,064 and 532 nm lasers at 350 Torr of N_2 ambient pressure and at $t_d = 1 \mu s$.

The temporal evolution of the electron density at different N_2 ambient pressures for the titanium plasmas generated by the two lasers at the wavelengths of 532 nm and 1,064 nm shows that the electron density is considerably

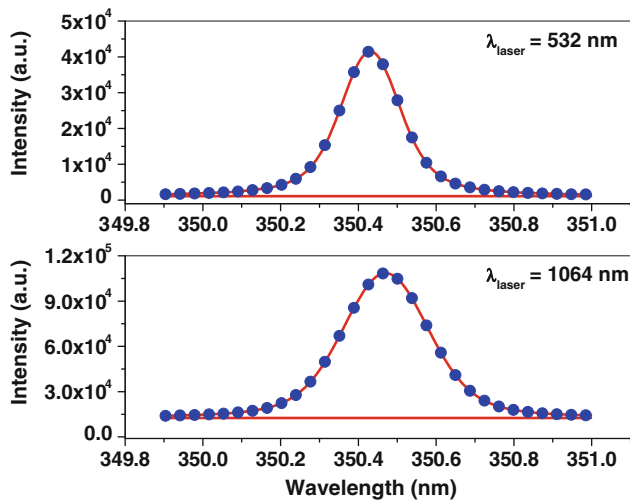


Fig. 9 Profile of the Ti II line at 350.49 nm (*dot line*) with its best fit (*solid line*) for the plasma generated by the 532 and 1,064 nm lasers at 350 Torr of N₂ ambient gas and for $t_d = 1 \mu\text{s}$

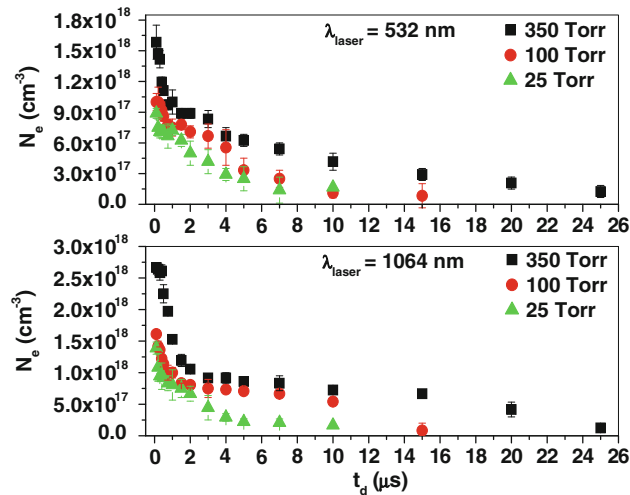


Fig. 10 Temporal variation in the electron density for the Ti plasma generated by 532 and 1,064 nm lasers at different pressure of ambient N₂ gas

high at the initial stage of the plasma, and then, it decreases quickly with the delay time as shown in Fig. 10. Therefore, the electron density ranged from about 2.8×10^{18} to $7.4 \times 10^{17} \text{ cm}^{-3}$ and from 1.78×10^{18} to $6.17 \times 10^{17} \text{ cm}^{-3}$ in the delay time range from 0.1 to 10 μs for plasmas produced by the 1,064 nm and 532 nm lasers, respectively, at atmospheric pressure of N₂. While at very low pressure (25 Torr), the density ranged from 1.39×10^{18} to $1.67 \times 10^{17} \text{ cm}^{-3}$ and from 8.89×10^{17} to $1.67 \times 10^{17} \text{ cm}^{-3}$ in the delay range from 0.1 to 10 μs for plasma produced by the 1,064 nm and 532 nm lasers, respectively. These values can be seen in Table 3.

Figure 11 shows the variation in the electron density with different pressures of N₂ ambient gas at different delay times for the titanium plasma generated by laser wavelengths of 532 nm and 1,064 nm. It can be noticed that the electron density increases with the pressure of the ambient N₂, and it decreases with increasing delay time.

6 Conclusions

From the present study, at lower ambient pressure values of N₂, the intensities of Ti spectral lines last only for a few hundreds of nanoseconds even not more than 500 ns at 15 Torr. As the ambient pressure is increased, the intensities of the lines can last for up to several microseconds and even reach about 25 μs at 760 Torr. However, it is observed that the intensities of the spectral lines increase with increasing ambient N₂ pressures, especially at the higher values of the ambient N₂ pressure where the intensities of the lines increase rapidly. Continuum radiation results from collisions of electrons with heavy particles, neutrals, and ions and is also due to recombination of the electrons with ions. Thus, it can be inferred that at the initial stage of the plasma near the ablated surface, there are a large number of electrons, ions, and neutrals in the excited states.

Table 3 Electron density values for plasma produced by both laser wavelengths at different delays

P (Torr)	Electron density $\times 10^{17} \text{ (cm}^{-1}\text{)}$											
	$t_d = 0.1 \mu\text{s}$		$t_d = 0.5 \mu\text{s}$		$t_d = 1.0 \mu\text{s}$		$t_d = 3.0 \mu\text{s}$		$t_d = 5.0 \mu\text{s}$		$t_d = 10 \mu\text{s}$	
	532 nm	1,064 nm	532 nm	1,064 nm	532 nm	1,064 nm	532 nm	1,064 nm	532 nm	1,064 nm	532 nm	1,064 nm
25	8.89	13.9	7.08	9.17	7.22	8.06	4.17	4.44	2.50	2.22	1.67	1.67
50	9.17	14.8	7.78	9.67	7.32	8.61	4.67	6.39	2.92	4.58	2.22	2.08
100	10.0	16.1	8.61	11.4	7.50	10.0	6.67	7.50	3.33	7.08	2.33	5.42
200	13.6	21.7	9.72	14.7	8.06	11.7	7.33	8.75	4.17	7.80	2.92	6.39
350	15.8	26.7	11.1	22.5	10.0	15.3	8.33	9.17	6.25	8.61	4.17	7.25
760	17.8	28.0	13.1	24.5	12.0	17.0	9.43	9.30	8.25	8.80	6.17	7.40

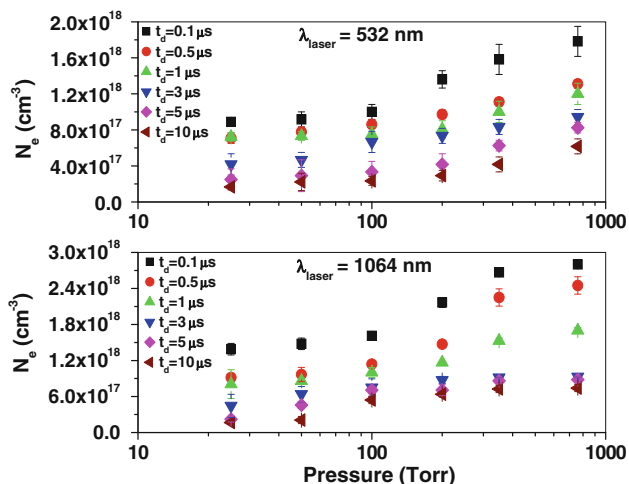


Fig. 11 Variation in the electron density for the Ti plasma generated by 532 and 1,064 nm lasers versus the ambient N_2 gas pressure determined for different time delays

The present work reveals that the intensities of Ti II spectral lines are much higher for the plasma generated by the 1,064 nm laser than those generated by the 532 nm laser for all pressures of ambient N_2 gas. We should mention that the higher intensity of spectral lines may be attributed to higher ablation of the sample. The mass ablation of the metal depends upon the thermodynamic and optical properties of the sample as well as on laser properties (wavelength, pulse duration, and irradiance). The effect of the ambient atmosphere (N_2) plays a dominant role in the mass ablation rate with the incident laser beam properties. Then, the changes in the properties of the plasma emission are due to the plume expansion changes, which are determined by the interaction of the plasma with the ambient atmosphere atoms.

Plasma temperature and density in the present study were considerably high at the initial stage of the plasma; then, they decreased quickly with time. It can also be noticed that the temperature and density increase with increasing pressures of ambient N_2 gas. The measured temperature ranged from about 1.66 to 1.1 eV and from 1.4 to 1.12 in the delay time range (0.1–10 μ s) for plasma produced by the 1,064 nm and 532 nm lasers, respectively, at atmospheric pressure of N_2 . At very low pressure (25 Torr), the corresponding temperature ranges were from 1.46 to 1.1 eV and from 1.22 to 1.01 eV in the delay ranges 0.1–3.0 μ s.

The electron density ranged from about 2.8×10^{18} to 7.4×10^{17} cm^{-3} and from 1.78×10^{18} to 6.17×10^{17} cm^{-3} in the delay time range from 0.1 to 10 μ s for plasma produced by the 1,064 nm and 532 nm lasers, respectively, at atmospheric pressure of N_2 ; at very low pressure (25 Torr), the corresponding density ranged from 1.39×10^{18} to 1.67×10^{17} cm^{-3} and from 8.89×10^{17} to 1.67×10^{17} cm^{-3} in the delay range from 0.1 to 10 μ s.

Acknowledgments Authors deeply thank Prof. H.-J. Kunze, Institut für Experimental Physik V, Ruhr Universität Bochum, Germany, whose advices, revising manuscript, and discussions during the progress of this work were invaluable.

References

1. J.A. Aguilera, C. Aragón, V. Madurga, J. Manrique, *Spectrochim. Acta, Part B* **64**, 993–998 (2009)
2. S. Liu, J. Zhu, Y. Liu, L. Zhao, *Mater. Lett.* **62**, 3881–3883 (2008)
3. A. Santagata, R. Teghil, A. De Giacomo, M. Dell’Aglia, G.P. Parisi, A. De Bonis, A. Galasso, *Appl. Surf. Sci.* **253**, 7792–7797 (2007)
4. O. Barthélemy, J. Margot, M. Chaker, M. Sabsabi, F. Vidal, T.W. Johnston, S. Laville, B. Le Droff, *Spectrochim. Acta, Part B* **60**, 905–914 (2005)
5. C. Aragón, J.A. Aguilera, *Spectrochim. Acta, Part B* **63**, 893–916 (2008)
6. A. De Giacomo, V.A. Shkhatov, G.S. Senesi, F. Prudeniano, *Appl. Surf. Sci.* **186**, 533–537 (2002)
7. S. Yalcin, D.R. Crosley, G.P. Smith, G.W. Faris, *Appl. Phys. B* **68**, 121–130 (1999)
8. A. Ciucci, M. Corsi, V. Palleschi, S. Rastelli, A. Salvetti, E. Tognoni, *Appl. Spectrosc.* **53**(8), 960–964 (1999)
9. *Pulsed Laser Deposition of Thin Films*, ed. by D. G. Chrisey, G.K. Hubler, (Wiley, New York, 1994)
10. D. Bauerle, *Laser Processing and Chemistry*, 2nd edn. (Springer, New York, 1996)
11. M. von Allmen, A. Blatter, *Laser-Beam Interactions with Materials*, 2nd edn. (Springer, New York, 1995)
12. E. D’Anna, G. Leggieri, A. Luches, M. Martino, A. Perrone, G. Majni, P. Mengucci, R. Alexandrescu, I.N. Mihailescu, J. Zemek, *Appl. Surf. Sci.* **86**, 170 (1995)
13. I.N. Mihailescu, N. Chitica, E. Gyorgy, V.S. Teodorescu, G. Marin, A. Luches, A. Perrone, M. Martino, J. Neamtu, *J. Mater. Sci.* **31**, 2909 (1996)
14. N. Chitica, E. Gyorgy, G. Adriana Lita, I.N. Mihailescu, D. Pantelica, M. Petrascu, A. Hatziapostolou, C. Grivas, N. Broll, A. Cornet, C. Mirica, A. Andrei, *Thin Solid Films* **301**, 71 (1997)
15. S. Eliezer, N. Eliaz, E. Grossman, D. Fisher, I. Gouzman, Z. Henis, S. Pecker, Y. Horovitz, M. Fraenkel, S. Maman, Y. Le-reah, *Phys. Rev. B* **69**, 144119 (2004)
16. S. Amoroso, G. Ausanio, R. Bruzzese, M. Vitiello, X. Wang, *Phys. Rev. B* **71**, 033406 (2005)
17. D. Scuderi, O. Albert, D. Moreau, P.P. Pronko, J. Etchepare, *Appl. Phys. Lett.* **86**, 071502 (2005)
18. L.V. Zhigilei, *Appl. Phys. A* **76**, 339 (2003)
19. E. Rolinski, *Surf. Eng.* **2**(1), 35 (1986)
20. A. Bharti, D.B. God, R.S. Sivakumar, A study of laser alloying of titanium alloys, in *Proc. ICALEO 88*, ed. by G. Bruck (1988)
21. S. Katayama, A. Matsunawa, A. Morimoto, S. Ishimoto, Y. Arata, Surface hardening of titanium by laser nitriding, in *Proc. ICALEO 83*, ed. by E.A. Metzbowler (1983)
22. M. Seiersten, Surface nitriding of titanium by laser beams, in *Proc. First Nordic Laser Material Processing conference*, ed. by B. Thorstensen (1988)
23. A. Walker, J. Folkes, W.M. Steen, D.R. West, *Surf. Eng.* **1**(2), 23 (1985)
24. T. Bell, W. Bergmann, J. Lanagan, P.H. Morton, A.M. Staines, *Surf. Eng.* **2**(2), 133 (1986)
25. H.S. Ubhi, T.N. Baker, P. Holdway, A.W. Bowen, The development of surface-modified microstructure in laser-treated titanium and titanium alloys, in *Proc. Sixth world conference on titanium*, France (1988)

26. V.M. Weerasinghe, D.R. West, J. de Damborenea, J. Mater. Process. Technol. **58**, 79–86 (1996)
27. L. Lavisse, M.C. Sahour, J.M. Jouvard, G. Pillon, M.C. Marco de Lucas, S. Bourgeois, D. Grevey, Appl. Surf. Sci. **255**, 5515–5518 (2009)
28. A.L. Thomann, E. Sicard, C. Boulmer-Leborgne, C. Vivien, J. Hermann, C. Andreazza-Vignolle, P. Andreazza, C. Meneau, Surf. Coat. Technol. **97**, 448 (1997)
29. E. Gyorgy, A. Perez del Pino, P. Serra, J.L. Morenza, Appl. Surf. Sci. **186**, 130 (2002)
30. D. Hoche, G. Rapin, J. Kaspar, M. Shinn, P. Schaaf, Appl. Surf. Sci. **253**, 8041 (2007)
31. Yu. Hanjiang, Fengjiu Sun, Jun Zhang, Curr. Appl. Phys. **9**, 227–233 (2009)
32. R. Lahoz, J.P. Espinos, G.F. de la Fuente, A.R. Gonzalez-Elipse, Surf. Coat. Technol. **202**, 1486–1492 (2008)
33. I. García, J.J. de Damborenea, Corros. Sci. **40**, 1411 (1998)
34. M.S. Lima, F. Folio, S. Mischler, Surf. Coat. Technol. **199**, 83 (2005)
35. J.M. Lackner, W. Waldhauser, R. Berghauser, R. Ebner, B. Major, T. Schoberl, Thin Solid Films **453–454**, 195 (2004)
36. C.Y. Lim, S.C. Lim, K.S. Lee, Tribol. Int. **32**, 393 (1999)
37. R.R. Manory, A.J. Perry, D. Rafaja, R. Nowak, Surf. Coat. Technol. **114**, 137 (1999)
38. H.C. Man, Z.D. Cui, X.J. Yang, Appl. Surf. Sci. **199**, 293 (2002)
39. B.S. Yilbas, J. Nickel, Wear **212**, 140 (1997)
40. P. Jiang, Surf. Coat. Technol. **130**, 24 (2000)
41. C. Langlade, A.B. Vannes, J.M. Krafft, J.R. Martin, Surf. Coat. Technol. **100–101**, 383 (1998)
42. E. Bemporad, M. Sebastiani, C. Pecchio, Surf. Coat. Technol. **201**, 2155 (2006)
43. E. Gyorgy, A. Perez del Pino, P. Serra, J.L. Morenza, Appl. Surf. Sci. **186**, 130 (2002)
44. A. Perez del Pino, P. Serra, J.L. Morenza, Thin Solid Films **415**, 201 (2002)
45. J.B. Price, J.O. Borland, S. Selbrede, Thin Solid Films **236**, 311 (1993)
46. R.I. Hedge, R.W. Fiordalice, E.O. Travis, P.J. Tobin, J. Vac. Sci. Technol. **B11**, 1287 (1993)
47. R.E. Krebs, *The History and Use of Our Earth's Chemical Elements: A Reference Guide* (2nd ed). (Greenwood Press, Westport, 2006). ISBN 0313334382
48. J. Emsley, "Titanium". *Nature's Building Blocks: An A-Z Guide to the Elements*. (Oxford University Press, Oxford, 2001). ISBN 0198503407
49. N. Casillas, S. Charlebois, W.H. Smyrl, H.S. White, J. Electrochem. Soc. **141**(3), 636–642 (1994)
50. Y.X. Leng, J.Y. Chen, P. Yang, J. Wang, A.S. Zhao, G.J. Wan, H. Sun, N. Huang, Surf. Coat. Technol. **201**, 1012–1016 (2006)
51. J.R. Davis, *Metals Handbook*. ASM International (1998). ISBN 08717-0654-7
52. J. Donachie, J. Matthew. *TITANIUM: A Technical Guide*. ASM International (2000). ISBN 08717-0686-5
53. H. Hegazy, H. Abd El-Ghany, S. Allam, Th El-Sherbini, Appl. Phys. B **110**, 509–518 (2013)
54. L. Fornarini, V. Spizzichino, F. Colao, R. Fantoni, V. Lazic, Influence of laser wavelength on LIBS diagnostics applied to the analysis of ancient bronzes. Anal. Bioanal. Chem. **385**, 272–280 (2006)
55. D.A. Cremers, L.J. Radziemski, Anal. Chem. **55**, 1252 (1983)
56. J.B. Simeonsson, A.W. Miziolek, Appl. Opt. **32**, 939 (1993)
57. M. Sabsabi, P. Cielo, Appl. Spectrosc. **49**, 499 (1995)
58. H.-J. Kunze, *Spectroscopy of Optically Thick Plasmas*, 3rd Workshop on Plasma and Laser Technology, Ismailia Oct 3–7, (1993) 31
59. H. Hegazy, Oxygen spectral lines for diagnostics of atmospheric laser-induced plasmas. Appl. Phys. B. Lasers Optics **98**, 601–606 (2010)
60. H.R. Griem, *Plasma spectroscopy* (McGraw-Hill Book Company, New York, 1964)
61. R.H. Huddleston, S.L. Leonard, *Plasma Diagnostic Techniques* (Academic Press, New York, 1965)
62. <http://www.nist.gov/>
63. C. Colón, G. Hatem, E. Verdugo, P. Ruiz, J. Campos, J. Appl. Phys. **73**, 4752–4758 (1993)
64. S.S. Harilal, C.V. Bindhu, R.C. Isaac, V.P. Nampoore, C.P. Vallabhan, J. Appl. Phys. **82**, 2140–2146 (1997)
65. H.C. Liu, X.L. Mao, J.H. Yoo, R.E. Russo, Spectrochim. Acta **B54**, 1607 (1999)
66. X. Zeng, X.L. Mao, S. Mao, J.H. Yoo, R. Greif, R.E. Russo, J. Appl. Phys. **95**, 816 (2004)
67. J. Hermann, C. Boulmer-Leborgne, D. Hong, J. Appl. Phys. **83**, 691–696 (1998)
68. J. Hermann, A. Thomann, C. Boulmer-Leborgne, B. Dubreuil, M. De Giorgi, A. Perrone, A. Luches, N. Mihailescu, J. Appl. Phys. **77**, 2928–2936 (1995)